# 7

# UV Laser Ablation of Polymers: From Structuring to Thin Film Deposition

Thomas Lippert

**Summary.** UV laser ablation of polymers is a versatile method to structure polymers with high resolution. The mechanism of ablation is often discussed controversially, but it is necessary to keep in mind that polymers are complex systems with a wide variety of properties that can influence the ablation mechanism. Analyzing the data, it appears that the ablation mechanism is a complex interrelated system, where photochemical and photothermal reactions are very important. The pressure jump, which is associated with the creation of small molecules and originates from both types of reaction, is also important for ablation. The importance of each effect is strongly dependent on the type of polymer, the laser wavelengths, the pulse length, and the substrate. UV laser ablation can also be utilized to deposit directly thin polymer films by PLD, but this is limited to certain polymers. Alternative laser-based techniques (LIFT) utilize the decomposition of a thin layer to transfer complete layers with high spatial resolution. This approach can be used to transfer pixels of sensitive materials to a substrate with a minimal thermal and UV load.

## 7.1 Introduction

### 7.1.1 Laser Ablation of Polymers

Laser ablation of polymers was first reported by Srinivasan et al. [1] and Kawamura et al. [2] in 1982. Since then, numerous reviews on laser ablation of a large variety of polymers and the different proposed ablation mechanisms have been published [3–11]. There is still an ongoing discussion about the ablation mechanisms, e.g., whether it is dominated by photothermal or photochemical processes.

Since its discovery, laser polymer processing has become an important field of applied and fundamental research. The research can be separated into two fields, the investigation of the ablation mechanism and its modeling and the application to produce novel materials or structures. Laser ablation is used as an analytical tool in *matrix-assisted laser desorption/ionization (MALDI)*

[12,13] and *laser-induced breakdown spectroscopy (LIBS)* [14] or as preparative tool for the deposition of thin films, e.g., by *pulsed laser deposition (PLD)* of synthetic polymers [15–17] (of inorganic films [18,19]), *matrix-assisted pulsed laser evaporation (MAPLE)*, which is a deposition technique that can be used to deposit highly uniform thin films [20], or *laser-induced forward transfer (LIFT)* [21,22].

There are several industrial applications for polymers in laser ablation, mainly for structuring, i.e., for the production of nozzles for inkjet printers [23] and to prepare via-holes in multichip modules through polyimide by IBM [24]. Laser ablation for other applications, e.g., fabrication of micro-optical devices [25] and microfluidic channels [26–29], are under development.

### 7.1.2 Polymers: A Short Primer

Polymers are macromolecules, which are synthesized from one or more different monomers using different types of polymerization, i.e., radical or ionic polymerization, polycondensation, polyaddition, and special cases such as copolymerization. To start the polymerization reaction, starters have to be applied in many cases, e.g., molecules that form a radical upon reaction that is initiated by temperature or light or even complex initiators and enzymes. The polymerization type has also a direct influence on the characteristics of the polymer, e.g., molecular weight and distribution, impurities, polymer structure (tacticity), or molecular form, and on the decomposition mechanism. The molecular weight, $M_{\mathrm{w}}$, of the polymer has a direct influence on the state of the polymer, i.e., low molecular weight polymers may still be liquids, while high molecular weight polymers are solids, which may even be insoluble in all solvents if the molecular weight is too high. The $M_{\mathrm{w}}$ subsequently influences the viscosity of the polymer (in the melt or solution), the glass transition temperature, $T_{\mathrm{g}}$, which is the temperature at which the polymer changes from the glass to rubber state, and possibly the melting and decomposition temperature. The $M_{\mathrm{w}}$ of a polymer is not one well-defined number, but a range of molecular weights is obtained from the synthesis, and normally an average is quoted. To be more precise, the polydispersity is used, which is the ratio of the weight average molecular weight to the number average molecular weight and an indication for the distribution of the molecular weights. In polymer chemistry, a Schulz–Flory distribution is often used to describe the variation of molecular weights. The polymer synthesis and structure of the monomer have a direct influence on the chain regularity/conformation of the polymer, which is also called tacticity. A polymer can have an atactic (random), iso or syndiotactic (ordered, see Fig. 7.1) structure, which again influences properties such as the $T_{\mathrm{g}}$. In the case of optical active monomers, optical active polymers may be obtained as pure D-, L-, or D-L (racemic) structure, which is common for biopolymers. Another aspect that is specifically important for the photon–polymer interactions is the possibility of polymers to be partially crystalline (never really complete, even if they are called single crystals), which results in

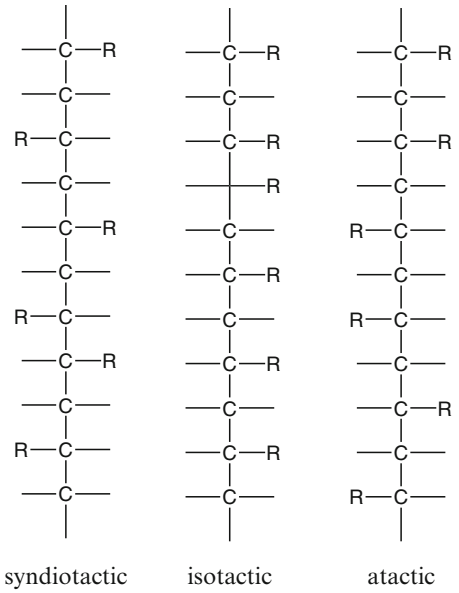


**Fig. 7.1.** Possible conformations of a polymer chain

light scattering (not absorption) in the polymer. Finally, it is also necessary to consider that most polymers cannot be vaporized (sublimed) intact and that many do not have a melting point prior to decomposition, which is the case for cross-linked polymers or many polyimides.

Most of these polymer characteristics can have, as described below, an influence on the ablation behavior of polymer, while the decomposition type is important for the ablation mechanism and the possibility to form thin films.

### Classification of the Decomposition Behavior

The decomposition mechanism of a polymer is a reasonable way to classify polymers for their behavior upon UV laser irradiation. Polymers which decompose into fragments are for example polyimides or polycarbonates (see Figs. 7.2 and 7.3). This method of classification is closely related to the synthesis of the polymers. Polymers that are produced by radical polymerization from monomers, which contain double bonds, are likely to depolymerize into monomers, while polymers that have been formed by reactions such as polycondensation will not depolymerize into monomers upon irradiation, but will be decomposed into different fragments. The second group cannot be used to produce films with the same structure or molecular weight as the original material with methods such as PLD.

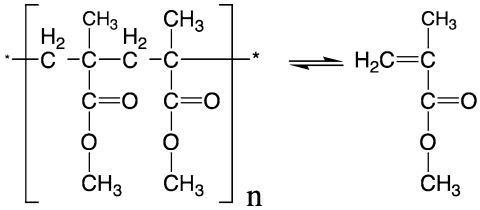

**Fig. 7.2.** Chemical structure of PMMA and its monomer

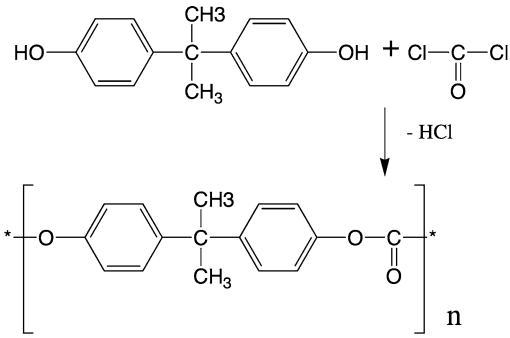

**Fig. 7.3.** Typical polycondensation reaction to form a polycarbonate

The different mechanisms may be described as:

*Depolymerization*

Some of these polymers show unzipping reactions (one radical on the polymer main chain yields several monomers) and have a ceiling temperature ($T_c$, above which the equilibrium between polymer and monomer is totally on the side of the monomer). A typical example is poly(methylmetacrylate) (PMMA, see Fig. 7.2), which has a ceiling temperature of 550 K and the zip length (the number of monomers originating from every chain end radical) is 6 at room temperature and ~200 above the glass transition temperature (378 K) of PMMA. Other examples of unzipping polymers are polystyrene and Teflon.

*Decomposition or Fragmentation*

Polymers that decompose into fragments are for example polyimides or polycarbonates. The reactions which are used to form these polymers are shown in Figs. 7.3 and 7.4. It is obvious that the monomers cannot be produced during decomposition, because one reaction product, e.g., $H_2O$ or HCl, is removed during polymerization.

These polymers show in the case of decomposition (thermally or photochemically) a tendency for a pronounced fragmentation into various small molecules, as shown for polyimide in Fig. 7.5. All the fragments shown have been detected by various analytical methods [30, 31].

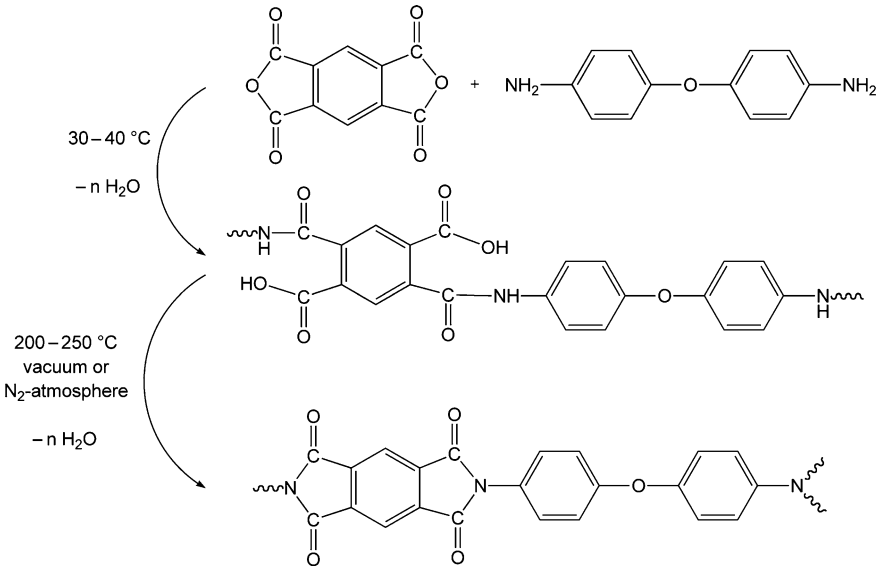


**Fig. 7.4.** Typical polycondensation reaction to form a polyimide

The large number of small decomposition products will results in a pronounced pressure increase inside the polymer matrix, which is important for ablation, as discussed in detail below.

## 7.2 Polymer Properties and Ablation

The influence of only some of the polymers properties, as discussed above, on ablation has not been studied in detail and only for the molecular weight several studies have been performed [32–35]. A clear influence of the molecular weight on the ablation rate was detected for doped PMMA (see Fig. 7.6) and has been assigned to the increased viscosity of the higher molecular weight polymer, which is clearly important for an ablation mechanism that shows clear indications of melting (see the ablation crater in Fig. 7.7).

A pronounced influence of the $M_w$ on the ablation behavior has also been detected for doped PMMA and polystyrene doped with Iodo-naphthalene. The formation of $Nap_2$ (=1,1-binaphthalene) as a product of irradiation has been analyzed by fluorescence spectroscopy, and a complex $M_w$ dependent behavior was detected that cannot be simply explained by the expected increase of viscosity for the higher molecular weight polymers. It seems that additional effects, e.g., higher ablation rates for lower $M_w$, the $T_g$, and bubble formation influence the rate of product formation [34, 35].

Another important parameter, which is especially important for technical polymers, is the presence of polymer additives or impurities that originate from the reaction (e.g., catalysts, starters). Additives to technical

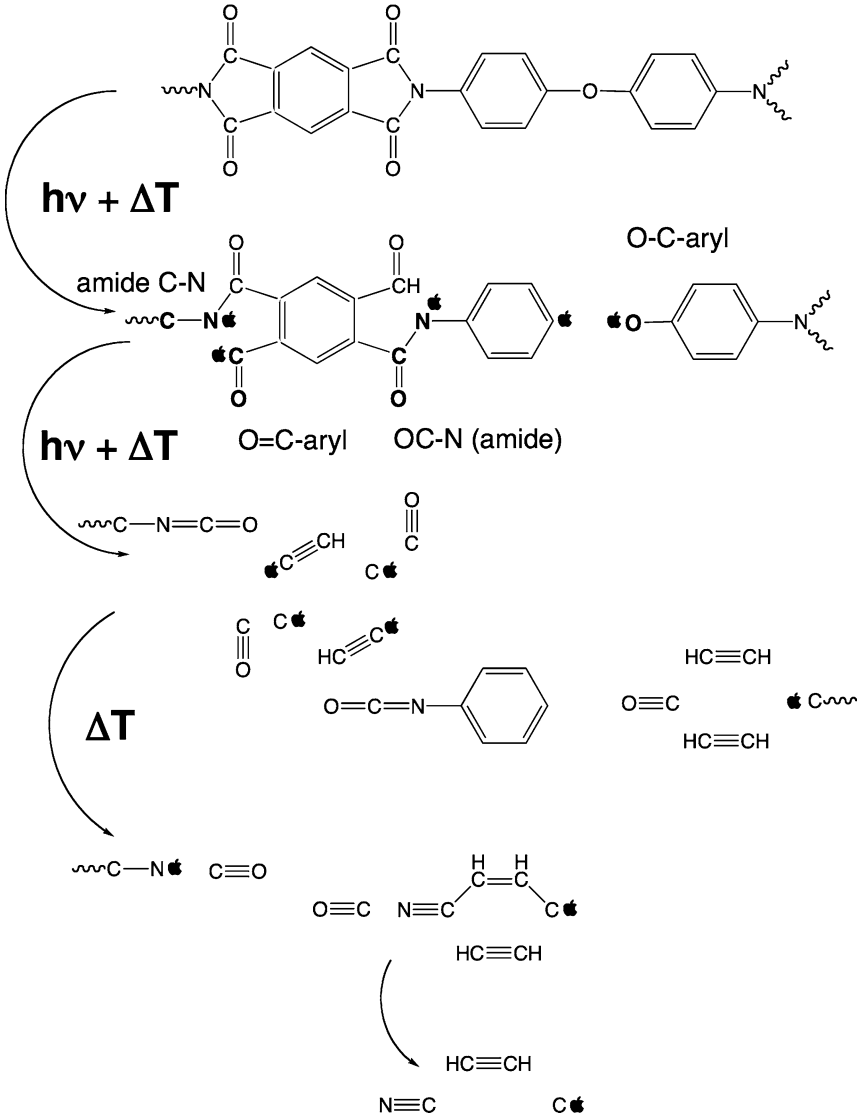


**Fig. 7.5.** Laser-induced decomposition/fragmentation of Kapton. All shown species have been detected. The ➠ denotes a radical, ion or broken bond

polymers such as antioxidants, UV absorbers, HALS (hindered amine light stabilizers), process and heat stabilizers for the stabilization of polymer recyclates, antistatics/antistatic agents, flame retardants, nucleating agents, oxygen absorbers, slip agents, carbon nanotubes/nanofilled thermosetting resins, optical brighteners/fluorescence indicators, plasticizers, silanes, silanes as bonding agents, silanes as cross-linking additives, antimicrobials, hydrophilic

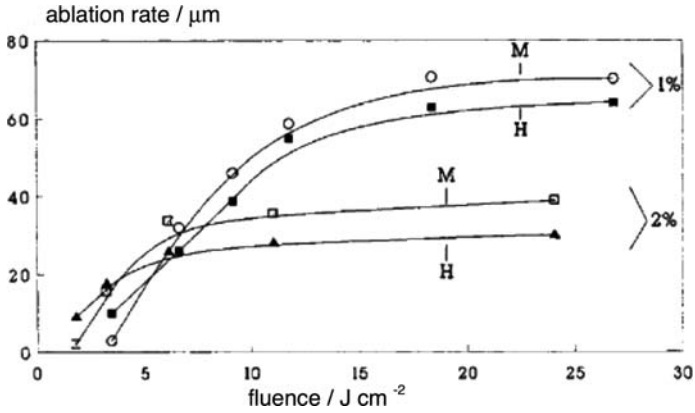


**Fig. 7.6.** Ablation rate for PMMA with an $M_w$ of 97,000 and 500,000 doped with different amounts of a triazene compound. Irradiation wavelength 308 nm

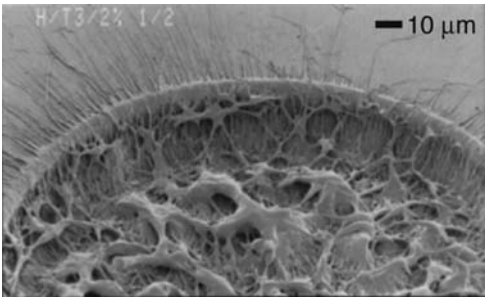


**Fig. 7.7.** Ablation crater in a triazene doped PMMA, with clear indications for melting during ablation. Irradiation wavelength 308 nm

additives, additives for content protection, photoselective additives, UV-Titan, titanium dioxide, and catalysts (not a complete list) are very common, and they may be inorganic or organic compounds. It is noteworthy that a common UV absorber (stabilizer), i.e., Tinuvin, can be used as dopant to induce effective ablation of PMMA at 308 and 350 nm [36, 37].

One possible effect, which can be observed for impurities in polymers, is the formation of microstructures, e.g., cones in a well-defined fluence range. The cone formation is due to the higher threshold fluence of ablation compared to the pure polymer, while the apex angle of the cones ($\Theta$) varies with the applied fluence ($F$) and ablation threshold ($F_0$) according to equation (7.1):

$$\Theta = 2 + \sin^{-1}\left[\frac{F_0\,(1 - R_0)}{F\,(1 - R\,(\Theta))}\right], \tag{7.1}$$

where $R_0$ and $R(\Theta)$ are the surface reflectivities for incidence angles of 90° (normal to the surface) and $\Theta$ degrees, respectively [38, 39]. Typical examples

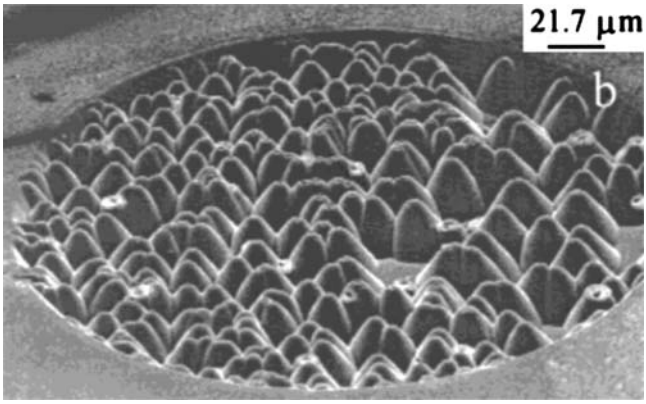


**Fig. 7.8.** Cone structures in a triazene polymer with a mixture of Si, O, and Cl on top of each cone. Irradiation wavelength 308 nm

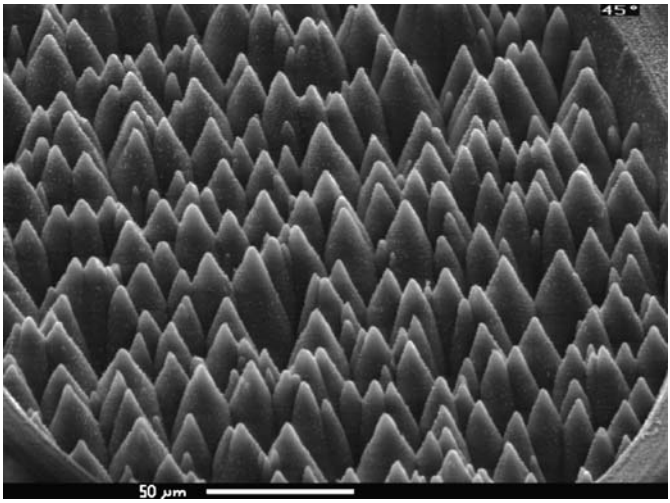


**Fig. 7.9.** Cone structures in a triazene polymer with a Ca-species on top of each cone. Irradiation wavelength 308 nm

of these cone structures are shown in Figs. 7.8 and 7.9. In Fig. 7.8 cone structures produced in a triazene polymer are shown, where on top of each cone Si, O, and Cl were detected, which indicates impurities from the synthesis which have not been removed completely during purification from the polymer [40].

In the case of Fig. 7.9 calcium was detected on top of each cone inside the ablation crater in polyimide sheets (Kapton$^{HN}$) [41]. According to the manufacturer Ca-stearate is used as antifriction compounds for the Kapton sheets.

The influence of chain end groups (see for example the end groups of the monomers in Figs. 7.3 and 7.4) on the ablation characteristics has not yet been analyzed in detail. End groups can/will influence the surface properties especially for low Mw polymers and may even change the absorption properties. Whether chiral polymers show specific features for ablation is also not known but is possible, if we consider that different microstructures have been observed for ablation with differently polarized light [42].

### 7.2.1 Polymer Names

It is of utmost importance not only to consider the methods of analysis for the data (e.g., single pulse vs. multi pulse, gravimetric vs. volumetric methods, such as AFM or profilometry) but also know which polymer has been used and whether it has been "prepared," e.g., purified to remove additives, and which polymer is really used. A good example for the latter is polyimide, which is/are probably the most studied polymer for ablation (due to its broad absorption which allows to use wavelength up to 355 nm for ablation). Polyimide is not one single polymer, but a class of polymers that consists of hundreds of different types. Even Kapton is not one polymer, but additionally letters such as HN, describe it in more detail, as almost a hundred different Kaptons exist. The properties of polyimides can even range from photosensitive to "photostable," which has a strong influence on the ablation characteristics (shown in Fig. 7.10). The ablation rates of two different polyimides have been analyzed by a quartz microbalance, and much higher ablation rates and lower threshold fluences have been detected for the photosensitive polyimide (Durimid) as compared to PMDA (a polyimide very similar to Kapton) [43, 44].

### 7.2.2 Polymers and Photochemistry

Photochemistry of polymers is a well-established field of research that also explains many features of laser ablation, especially in the low fluence range. Incubation of PMMA for example is based on the same photochemical processes, which result in photoyellowing of PMMA. This originates from the formation of double bonds in the polymer chain (chain end and in-chain). The formation of the double bonds is due to a classical photochemical reaction, i.e., the Norrish type I or α-cleavage, which can be described as the homolytic breaking of a bond next to a double bond with a heteroatom (C=O). This reaction creates several small reaction products, i.e., CO, $CO_2$, $CH_4$, $CH_3OH$, and $HCOOCH_3$, which have been all detected for photodecomposition and laser ablation of PMMA [30, 31]. Subsequent reactions after this reaction create the double bonds and the monomer (shown in Fig. 7.11). It is also noteworthy to mention that the monomer is the exclusive product from thermal decomposition of PMMA ($T >$ ceiling temperature) which is detected for $CO_2$ laser ablation, while only a small amount of monomer, i.e., ≈1% for 248 nm irradiation and ≈18% for 193 nm irradiation [45, 46] is detected for UV laser ablation. The rest of the products are the small products and polymer fragments.

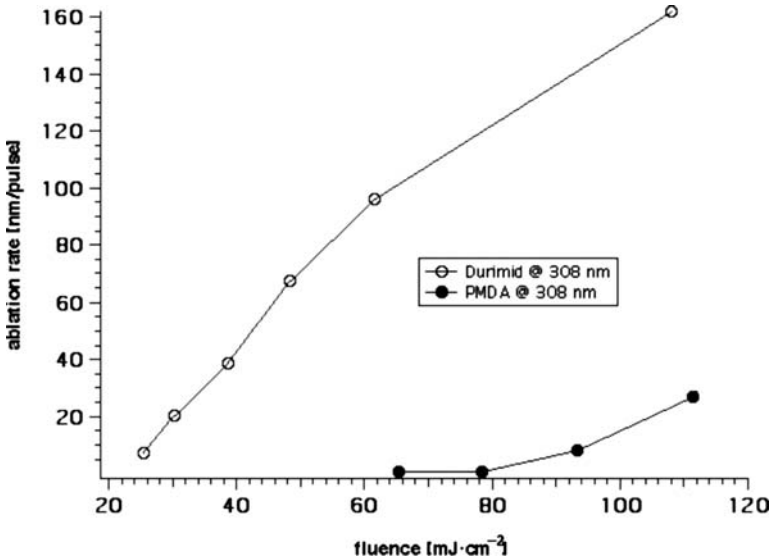


**Fig. 7.10.** Ablation rates of a photosensitive polyimide (Durimid) and PMDA (Kapton like). Irradiation wavelength 308 nm

### 7.2.3 Fundamental Issues of Laser Ablation

For an understanding of polymer ablation the main ablation parameters have to be explained and their definition have to be discussed in detail. Also the most frequently proposed ablation mechanisms and models will be discussed.

#### Ablation Parameters

The main parameters that describe polymer ablation are the *ablation rate*, $\mathrm{d}(F)$, and the *ablation threshold fluence* $F_{\mathrm{th}}$, which is defined as the minimum fluence where the onset of ablation can be observed. A third important parameter is the *effective absorption coefficient*, $\alpha_{\mathrm{eff}}$, which yields information on the mechanisms that take place in the ablation process when compared to the *linear absorption coefficient*, $\alpha_{\mathrm{lin}}$, that is measured on thin un-irradiated polymer films.

The ablation process is often described by the following equation [47, 48]:

$$\mathrm{d}(F) = \frac{1}{\alpha_{\mathrm{eff}}} \ln\left(\frac{F}{F_{\mathrm{th}}}\right) \tag{7.2}$$

Also the method as to how the ablation parameters are acquired can have a pronounced influence on the results. The ablation rate can be defined either as the depth of the ablation crater after one pulse at a given fluence, or as the slope of a linear fit of a plot of the ablation depth versus the pulse

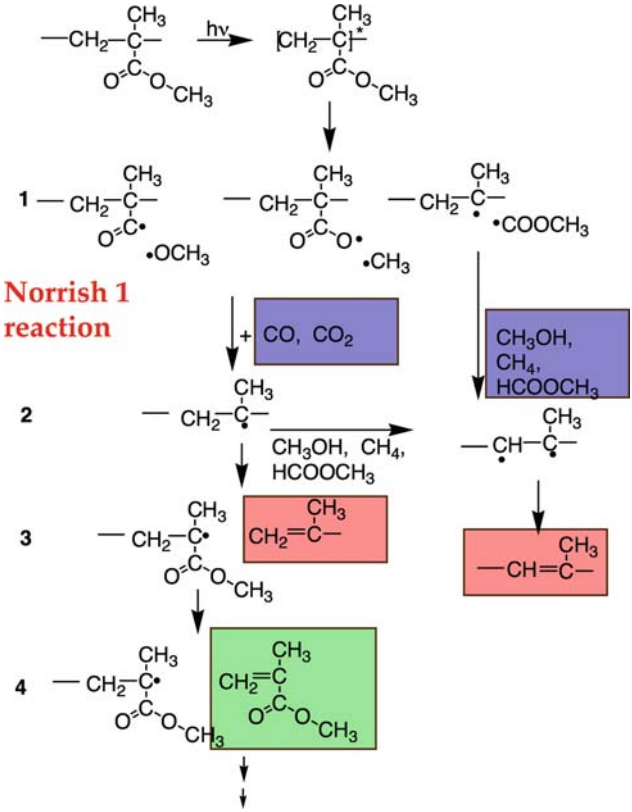


**Fig. 7.11.** Photochemical decomposition pathway of PMMA

number for a given fluence. Very different ablation rates can result from the two different measurement methods. This is especially the case for materials where ablation does not start with the first pulse, but after multiple pulses, or if the ablation crater depth after one pulse is too small to be measured. The process that occurs if ablation that does not start with the first laser pulse, is called *incubation*. It is related to the physical or chemical modifications of the material by the first few laser pulses, which results often in an increase of the absorption at the irradiation wavelength [49, 50], e.g., the formation of double bonds in *poly(methylmetacrylate) (PMMA)*. Incubation is normally only observed for polymers with low absorption coefficients at the irradiation wavelength. The typical appearance of incubation in a plot of the ablation depths vs. pulse number is shown in Fig. 7.12.

The method applied to measure the depth of the ablated area or the removed mass can also have an influence on the ablation parameters. If profilometric measurements (optical interferometry, mechanical stylus [51] or atomic force microscopy [52]) are used to calculate the ablation rate, a sharp ablation

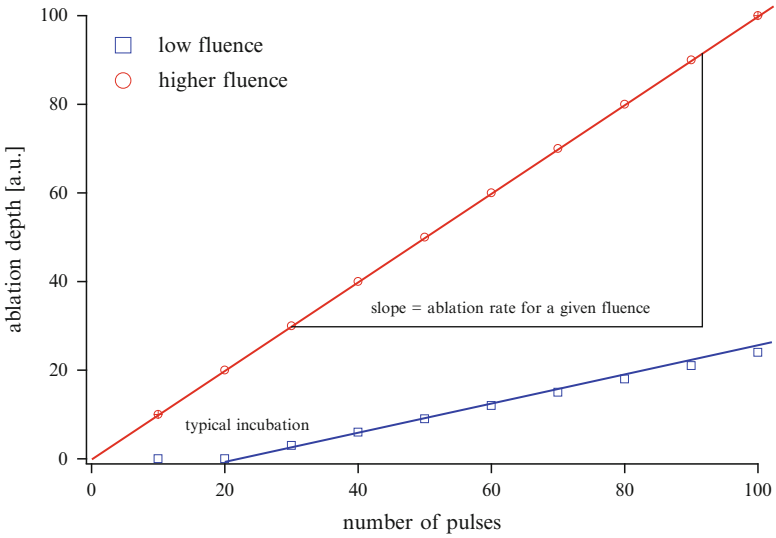


**Fig. 7.12.** Plot of ablation depth vs. pulse number, which is used to determine the ablation rate for a given fluence. The typical feature of incubation, i.e., ablation starts only after a certain number of pulses is shown for the lower curve

threshold can be defined. This is also supported by reflectivity [53] and acoustic measurements [54]. In mass loss measurements, such as mass spectrometry or with a *quartz crystal microbalance (QCM)*, a so called *Arrhenius tail* [55] has been observed for certain conditions. The Arrhenius tail describes a region in the very low fluence range, where a linear increase of detected ablation products is observed, which is followed by a much faster increase, that coincides with the removal rates of the profilometric measurements [43].

Even if these different approaches are taken into account, it is often the case, that the ablation rate cannot be defined with a single set of parameters. Therefore, one set of parameters has to be defined for each fluence range in which different processes dominate the ablation process and thereby influence the ablation rate. In Fig. 7.13 the dependence of the ablation rate on the irradiation fluence is illustrated as a generic scheme, which is typical for most polymers. The intersection of the gray extensions of the schematic ablation rates (*black lines*) with the $x$-axis of the ablation rate vs. irradiation fluence plot is the threshold fluence and varies for each fluence range. Also a different effective absorption coefficient can be defined for each region.

Three fluence ranges are visible, which can be characterized as follows:
*Low fluence range:*

- From this fluence range, the ablation threshold fluence is normally defined
- Incubation can be observed at these low fluences

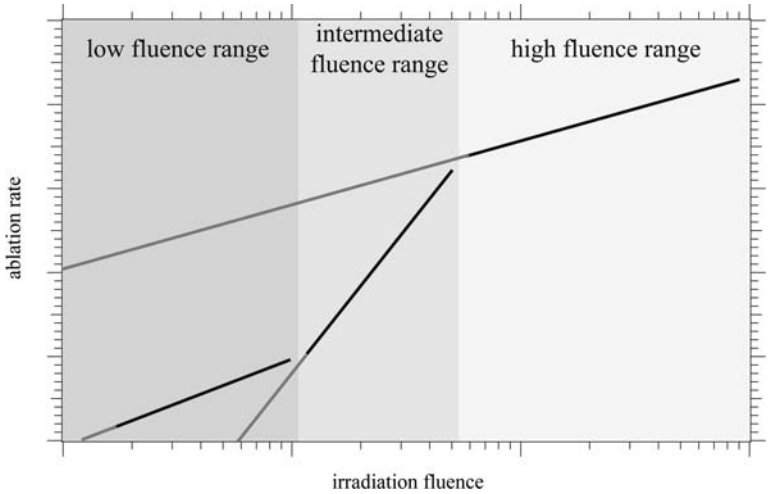


**Fig. 7.13.** Schematic plot of the three fluence ranges which are typically observed for polymers. The three ranges are indicated with different *shades of gray*

*Intermediate fluence range:*

- Increase of the slope of the ablation rate, which is caused by a more efficient decomposition of the polymer. Energy that has been gained from an exothermic decomposition of the polymer can also increase the ablation rate

*High fluence range:*

- The incident laser light is screened by solid, liquid, and gaseous ablation products and the laser produced plasma. This leads to similar ablation rates for many polymers [5] at high fluences

### 7.2.4 Ablation Mechanism

It is therefore of great importance not only to consider the values for the different ablation parameters, but also information about the technique of analysis and for which fluence range they are valid. An interpolation to values beyond the measurement range is also not advisable, as not all three ranges have to be present for all polymers and irradiation condition.

Even after 25 years of research in the field of laser polymer ablation, there is still an ongoing discussion about the ablation mechanisms, e.g., whether in addition to these mechanisms, photothermal processes, photochemical reactions, or even photophysical and mechanical processes are important.

If we summarize the experimental data and known reactions and products, then the following trends can be established:

- Absorption of the UV laser photons can and will result in direct bond breaking with a certain quantum yield ($<1$). The photon energy not

resulting in bond breaking is transferred to the polymer matrix ➠ increase of T.

- Direct bond breaking is very fast (fs-ps) compared to the time scale of typical UV laser ablation (excimer lasers with ns pulse duration) ➠ primary decomposition products can also be decomposed directly by the laser photons (also possible for secondary products, etc.)
- The reactions create different structures with different absorption properties and different quantum yields (QY) for their further decomposition. Energy can be released from exothermic decomposition reactions (up to $\mathrm{kJ\,g^{-1}}$) ➠ increase of $T$.
- Small reaction/decomposition products are formed ➠ increase of $p$.
- The increase of $T$ results in thermal decomposition of the polymer (can be quite fast as high temperatures may be reached in short time scale) ➠ increase of $p$.
- The fast increase of $T$ can also increase the QY and subsequent reactions (unzipping: for PMMA 6 monomers at RT and over 200 above $T_{\mathrm{g}}$) ➠ increase of $p$.
- Ablation starts when a certain number of bonds are broken in a volume element (before: decomposition/incubation) ➠ delayed ablation of a *modified* (not original) polymer.
- All of these processes are dependent on the polymer ➠ very complex ablation mechanism.

This complex behavior explains why the ablation mechanism has been and is still controversial. It is very difficult to separate the products of thermal and photochemical decomposition (they are often very similar), but ablation products must be considered (remember very different products for thermal/photochemical reaction of PMMA). Many different reactions are possible, which makes it difficult to model the complete process. Many constants of the polymer are temperature dependent and partly unknown for the possible high temperatures (and high heating rates present for laser irradiation). It is also difficult to establish an energy balance, because for many reactions the parameters are not known, and energy is carried away by the ablation products, which is difficult to measure (model correctly).

## Modeling of Laser Ablation

It is generally accepted that for ns laser pulses, the energy of the laser photons is used for electronic excitation in a first step. The following steps are still under discussion and the different *models* can be summarized as follows:

*Photothermal:* The electronic excitation is thermalized on a ps timescale, which then results in thermal bond breaking [56–60].

*Photochemical:* Electronic excitation results in direct bond breaking [5, 47, 61–63].

*Photophysical:* Both thermal and nonthermal processes play a role. Two independent channels of bond breaking [64, 65] or different bond breaking

energies for ground state and electronically excited states chromophores are applied [66,67] in this model. It is most adequate for short laser pulses in the ps and fs range [68].

Another way to distinguish the different models is by separating them into *surface* and *volume* models. In the volume models, the different processes that eventually result in ablation take place within the bulk of the material. In the surface models, the processes that are responsible for the material removal take place within a few monolayers below the surface. The different models can be described as follows:

*Photochemical surface models:* valid for long pulses and/or higher irradiation fluences [69].

*Thermal surface models:* These models are mainly developed for metal ablation and do not consider the sharp ablation threshold, but can describe the occurrence of an *Arrhenius tail* [59,60,65,70].

*Photochemical volume models:* These models describe a sharp ablation threshold and a logarithmic increase of the ablation crater depth with the number of laser pulses, but the *Arrhenius tail* is not accounted for [3,5,47, 61,62]. A linear dependence can be described with models that consider the motion of the ablation front, but ignores the screening effects caused by the plasma plume.

*Thermal volume models:* These models are often oversimplified by neglecting the movement of the solid-gas interface and result therefore in very high temperatures [55,58].

*Volume photothermal model:* In this model by Arnold and Bityurin [71], a thermal surface model and a photochemical volume model have been combined. In this model it is assumed, that photothermal bond breaking takes place within the bulk polymer. When a density of broken bonds reaches a critical value, ablation begins. This model can account for sharp ablation thresholds and Arrhenius tails.

A new *coarse-grained chemical reaction model (CGCRM)* has been proposed by Garrison et al. [72,73]. In this model a kinetic Monte Carlos approach that includes a probabilistic element is used to predict when reactions occur. It is thereby possible to avoid the use of a chemically correct interaction potential. The CGCRM uses known chemical reactions along with their probabilities and exothermicities for a specific material to estimate the effect of chemical reactions on the ablation process.

The coarse grained molecular dynamics model was developed to study the role of thermal, mechanical and chemical reactions in the onset of the ablation process of PMMA [74–79]. In this model, the laser energy is absorbed in different ways, i.e., pure heating and Norrish type I and II reactions. Mechanical stresses and pressures are dominant for very short pulses in the stress confinement regime and can initiate ablation by a mechanical breakdown of the polymer in the case of pure heating. For longer pulse lengths, the ejection process is mainly thermally activated. This can be well described with thermal models based on thermally activated bond braking processes. The presence

of small molecules and gaseous products cannot be accounted for by a purely thermal mechanism. A modeling of the photoablation channels requires a two-step ablation model that incorporates the effect of photolysis of the polymer and the creation of new species, which is then followed by a thermally activated removal step. The breathing sphere model was enhanced by Garrison et al. [80–83] to allow the photons to break a bond in the molecule and to describe subsequent abstraction and recombination reactions. The model was initially applied to chlorobenzene, where good correlation with experimental data was found.

The new concept that arises from these calculations is the difference in the temporal and spatial deposition of the available energy in photochemical and photothermal mechanisms. This concept provides the foundation to make specific comparisons with experiment and to explain experimental results as summarized below:

- It was found that photochemical reactions release additional energy into the irradiated sample and decrease the average cohesive energy and thereby decrease the value of the ablation threshold. The yield of emitted fragments becomes significant only above the ablation threshold.
- The presence of a shockwave with a high initial velocity, large clusters in the plume, and high velocities of particles in the plume are explained by the fast rise of energy deposition in time from 20 to 150 ps.
- The chemical reactions that take place above the surface after the laser pulse on longer timescales explain the higher background density in the plume with photochemical ablation than observed for photothermal ablation.
- The presence of a combination of a thermal mechanism below the ablation threshold and a volume ejection mechanism above the threshold explains why non-volatile products like HCl and the matrix are only observed below threshold and all products are observed above threshold.
- The absence of heat deposited below ∼1.5 times the penetration depth may help to explain the cold etching process in far UV photoablation as is used commercially in the corrective eye surgery, LASIK.

The different models include many material parameters and several of these parameters are obtained from fitting of experimental data, and have to be adjusted to fit each polymer [9, 84].

In general it can be said, that polymers that show a photochemical ablation behavior at the irradiation wavelength would be preferable for structuring, as the damage of the surrounding material due to a thermal processes is minimized and less carbonization is observed. A conversion of the polymer into gaseous products is also of advantage, as no or only minor amounts of ablation products are redeposited on the structured surface and additional cleaning procedures may not be necessary.

### 7.2.5 Doped Polymers

#### Motivation

If we consider that the absorption of the laser photons is the basis for UV laser ablation with ns pulses and that many polymers absorb only at wavelengths <240 nm then it appears logical that methods were tested to extend the absorption of polymers by doping and therefore the number of applicable lasers. The ablation of doped polymers has been reviewed in 1997 by Lippert et al. [85] and the polymers and the ablation mechanism were classified according to the absorption properties of the absorber-polymer system. The properties changed from systems, where only the dopant is absorbing, to systems, where absorption occurs only in the polymer. It was suggested, that ablation results from a mixture of processes, that originate from the polymer and the dopant. The properties of the dopant result in processes that can dominate the ablation mechanisms.

An important factor is whether the dopant is decomposing or not. A photolabile dopant, that decomposes into gaseous products leads to pronounced surface swelling at low irradiation fluences, while this behavior is much less pronounced for "photostable" dopants. Thermoelastic stress can also be induced in the polymer below the ablation threshold fluence by localized heating and thermal expansion of the polymer. This stress is then released in acoustic waves and thermal conduction into the surrounding material. The resulting transient and quasi-static thermoelastic stresses can lead to material damage and even material ejection. At high fluences, very high ablation rates [33] can be achieved, but with the drawback of pronounced surface melting. In the case of photostable dopants, less surface swelling, lower ablation rates, and structures with higher quality are observed.

For all doped systems, it has to be considered that the amount of dopant is limited (typically ≤10 wt.%) and that polymer properties such as $T_g$ may change (to lower values).

Different dopants were added to PMMA to investigate the ablation mechanism during UV irradiation. The dopants that were used ranged from polyaromatic compounds to compounds that contained photochemical active groups [85].

One group of dopants that was tested contains the triazene group (–N=N–N), as they are photochemically well studied [86–88] and also release a large amount of nitrogen when they are photochemically decomposed. Pronounced swelling has been observed by SEM analysis of the ablation craters at low irradiation fluences (see Fig. 7.14), which is caused by gaseous products produced by the decomposition of the photolabile dopants. It has been suggested that the released nitrogen and other gaseous ablation products act as carriers for larger ablation fragments.

With increasing fluence and dopant concentration, high ablation rates of up to 80 µm can be achieved, but pronounced signs of surface melting are

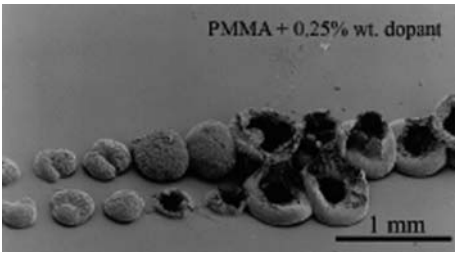


**Fig. 7.14.** Irradiated PMMA with different dopant concentration after irradiation with 308 nm. PMMA with 0.25 wt.% triazene was used for ablation with one laser pulse per position. The irradiation fluence increases from left to right. Pronounced swelling and bubble formation is visible

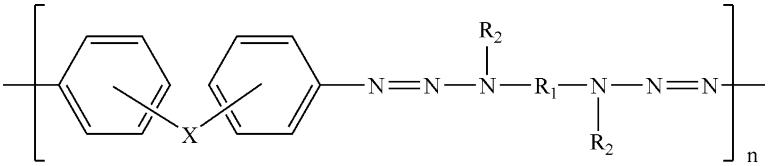


**Fig. 7.15.** Chemical structure of the triazene polymers

always visible [33] (see Fig. 7.7), which is an indication for the presence of a photothermal mechanism. A possible reason for these pronounced thermal effects could be that the maximum amount of dopant that can be added to the polymers is ≈10%, which limits achievable temperatures (energy/volume).

### 7.2.6 Designed Polymers: Triazene Polymers

New polymers have been developed to further improve the quality of the ablation process, i.e., to achieve higher ablation rates, lower threshold fluences, and better quality structures with no surface contamination and pronounced modification of the polymer. One approach was to incorporate the triazene unit into the polymer backbone. A unique feature of these triazene polymers (TP, chemical structure shown in Fig. 7.15) is the possibility to adjust the absorption maximum by varying the "X"-component in Fig. 7.15 [89]. The absorption maximum of such triazene polymers can be tuned from 290 to 360 nm and maximum linear absorption coefficients of up to $200,000\,\mathrm{cm}^{-1}$ at 308 nm can be reached.

In the absorption spectra for two different triazene polymers with $X = O$, $R_1 = (CH_2)_6$, and $R_2 = CH_3$ or $R_2 =$ t-butyl (shown in Fig. 7.16), two distinct absorption maxima can be distinguished. The $R_1$ and $R_2$ groups change the properties such as $T_g$, film forming and chromophore density. The absorption maximum around 200 nm can be assigned to the aromatic system, while the maximum around 330 nm corresponds to the triazene unit [90]. The absorption

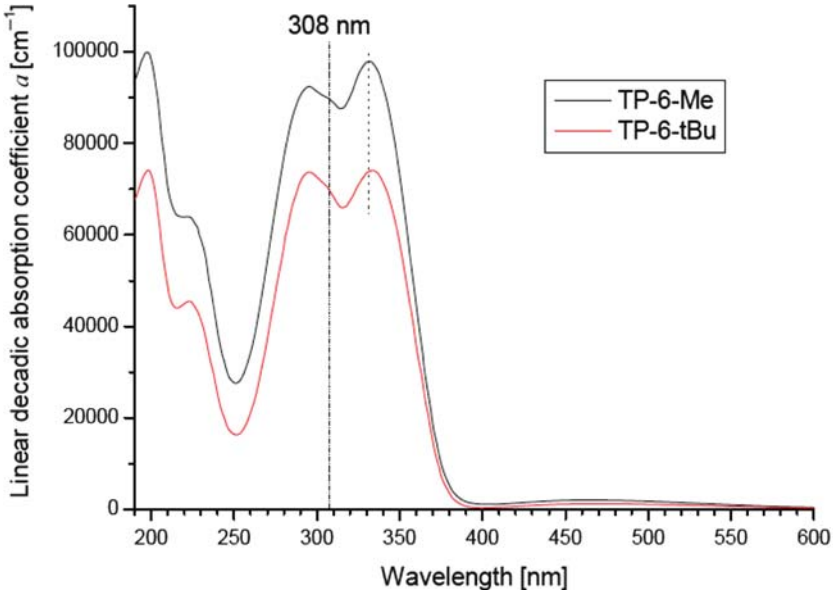


**Fig. 7.16.** Absorption spectra for two different triazene polymers with different chromophore density

coefficient of the triazene band can be influenced by $R_2$, i.e., with increasing bulkiness of the group the chromophore density decreases (as shown in Fig. 7.16 for Me vs. *t*-butyl). The two well-separated absorption maxima allow an excitation of different chromophores with different irradiation wavelengths such as 193, 248, and 308 nm, and thereby allow the study of their influence on the ablation behavior.

Higher ablation rates were measured for irradiation wavelengths that excite the triazene system (266, 308, and 351 nm) compared to the ablation rates for shorter wavelengths (248 and 193 nm) [6]. Also a clear and well defined ablation threshold fluence of 25 mJ cm$^{-2}$ ($\pm$5 mJ cm$^{-2}$) is observed for a TP at an irradiation wavelength of 308 nm, while for irradiation with 248 nm a much broader range, 16–28 mJ cm$^{-2}$ has been measured [90]. For irradiation at 248 nm, carbonization of the polymer was detected upon irradiation, whereas the surface of the polymer remained unchanged after several laser pulses for irradiation with 308 nm [91]. This is also an indication for the different ablation mechanisms at the irradiation wavelengths.

The triazene polymers are also well suited as probes for the ablation mechanism. Mass spectrometry was used to study the ablation products and to determine the different ablation mechanisms at the different irradiation wavelengths [92–94]. All decomposition products were identified with time resolved mass spectrometry for 248 nm and 308 nm irradiation. The proposed decomposition pathway for 308 nm irradiation is shown in Fig. 7.17, but similar

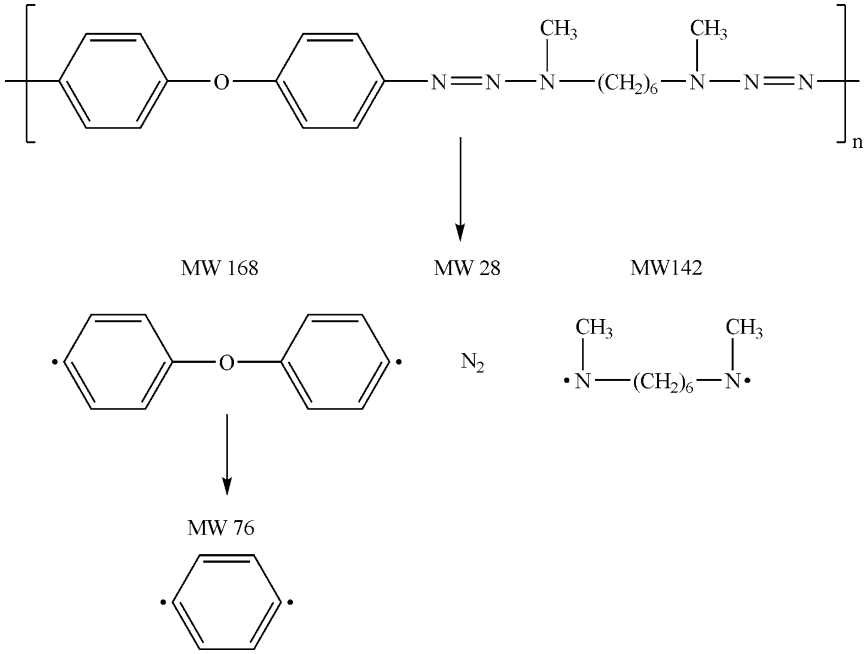


**Fig. 7.17.** Decomposition pathway for a TP measured by TOF-MS after irradiation with 308 nm

products were also observed for a thermal decomposition [87]. A clearer indication for the presence of a photochemical mechanism for 308 nm irradiation was given by the time-of-flight mass spectrometry (TOF-MS) data. Three different species of nitrogen were detected in the ablation plume (shown in Fig. 7.18): a very fast ground state neutral with up to 6 eV of kinetic energy, a slower ground state species with a broad energy distribution, which is most probable a thermal product, and a metastable (excited) neutral $N_2$ species that can only be created by an electronic excitation [95] because temperatures corresponding to this energy would be completely unreasonable.

It is interesting to compare the time of flight data and corresponding energies of the triazene polymer with data obtained for a polymer, i.e., Teflon, where we expect an unzipping and which also has a ceiling temperature (pronounced thermal decomposition pathway). In Fig. 7.19 the time of flight curve for the main product of Teflon decomposition, $C_2F_4$ with a mass of 100 amu, is shown for irradiation at 248 nm. A single curve is obtained which can be modeled by Maxwell Boltzmann distribution. The temperature, which is obtained from the analysis, is 987 K that is very reasonable compared to the temperature of 630 K for which the onset of unzipping is expected. The clear difference between the triazene polymer and Teflon confirm, again, the importance and influence of the material on the ablation mechanism.

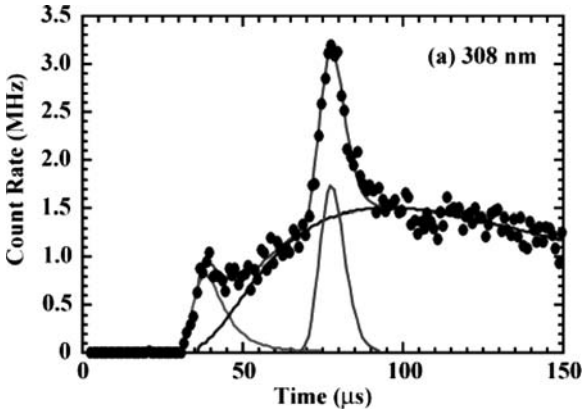


**Fig. 7.18.** Time of flight curves of the main product of decomposition of the triazene polymer, i.e., $N_2$. The irradiation wavelength was 308 nm with a fluence of 200 mJ cm$^{-2}$

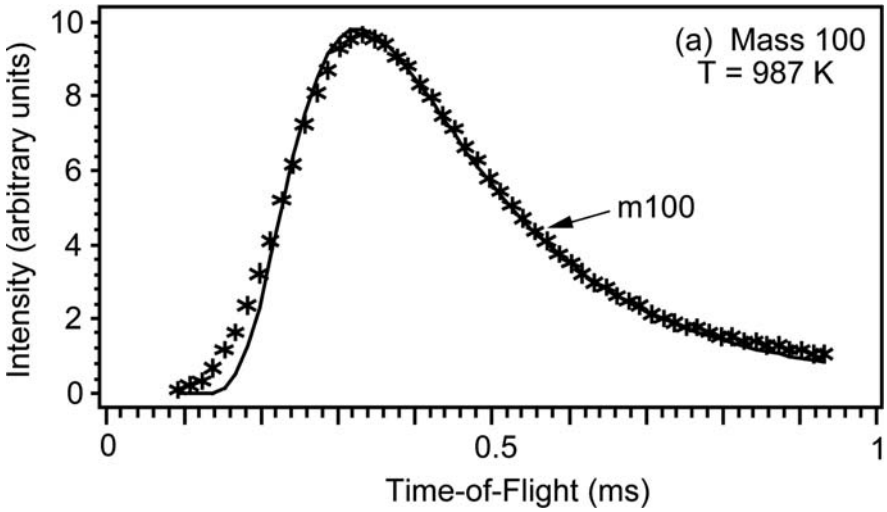


**Fig. 7.19.** Time of flight curve for the emission of the Teflon monomer for irradiation at 2 J cm$^{-2}$ at 248 nm. The dark line shows a curve fit to a Maxwell Boltzmann distribution at a temperature of 987 K

Another method, which can be used to determine the ablation mechanism, is ns-interferometry. The ablation process could take place on a longer time scale (depending on the temperature) for a photothermal processes than for a photochemical reaction. First, swelling is observed and that is followed by etching [96, 97], e.g., as discussed for a polyimide at 351 nm irradiation. This etching takes place on a microsecond time scale, which is much longer than the 30 ns excimer laser pulse. For the triazene polymer on the other hand the

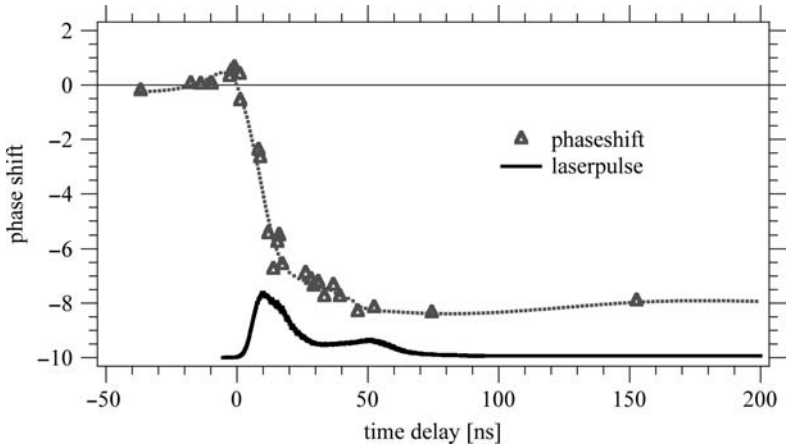


**Fig. 7.20.** Interference measurement for a triazene polymer during irradiation with 308 nm. The black curve represents the laser pulse, while the gray line corresponds to the phase shift, which is related to the ablation depth

etching starts and stops with the ablation laser pulse [98, 99] (see Fig. 7.20), which is again a clear indication for a photochemical process.

Irradiation experiments in the near-IR range at 800 nm with pulses in the pico- and femtosecond range were also performed. For femtosecond pulses, a lower ablation threshold fluence was found than for picosecond pulses, which indicates the presence of a thermal mechanism [100]. Also no complete removal of a thin triazene polymer film from a glass substrate was possible with 100 fs pulses. These short pulses in the near-IR do not yield much better results and are therefore no alternative to UV ablation [101].

The influence of the location of the predetermined "decomposition" site of in the polymer has been tested by incorporating the triazene unit into the side chains. The obtained ablation structures were less defined, and more pronounced thermal effects were observed [102]. Investigation of the polymer "between" the individual triazene units suggest that a higher triazene density results in better ablation results [7].

In Fig. 7.21 the ablation threshold fluences are plotted versus the polymer weight per triazene unit for TP1, two polyurethane polymers with the triazene unit in the polymer backbone (PUH-T1, PUH-T2) [103], two polyacrylates with the triazene unit in the polymer side chain (T-PAc1, T-PAc2) [102], two different triazene polymers with malonyl ester groups in the side chains (TM1 and TM2) [7] and a polyurethane polymer with the triazene unit in the side chain (PU-NO) [104]. A sudden increase of the ablation threshold fluence can be observed at about 285 amu/(triazene group) from ∼25 to ∼70 mJ cm$^{-2}$. Polymers above this jump have a higher ablation threshold fluence, as more bonds have to be broken to remove the larger remaining polymer fragments. Below or above this step, the ablation threshold fluence remains more or less

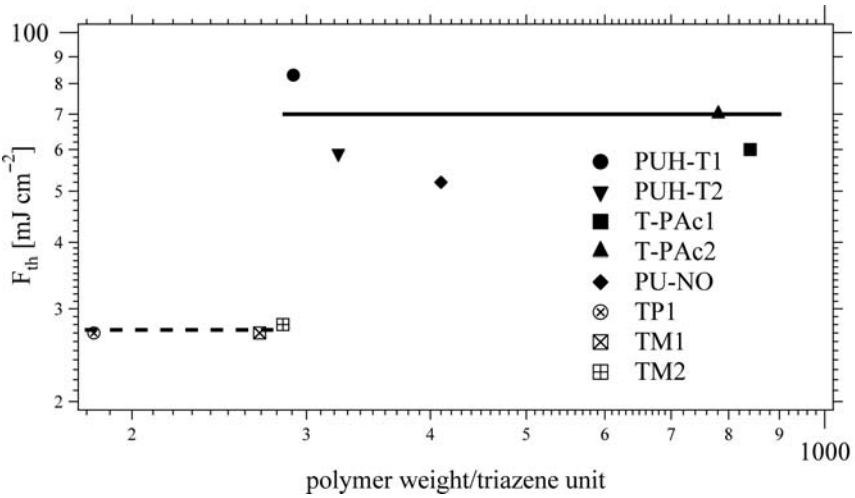


**Fig. 7.21.** The ablation threshold fluence versus polymer weight per triazene unit is shown for various triazene polymers. The two lines in the plot are shown as guidelines

constant, independent of the polymer weight per triazene unit. Why this sharp step is observed is not yet clear and must be studied in more detail.

### 7.2.7 Comparison of Designed and Commercially Available Polymers

Compared to commercially available polymers such as polyimides or other designed polymers, e.g., polyesters, the triazene polymers showed the highest ablation rates (up to 250 nm per pulse for 100 mJ cm$^{-2}$ compared e.g., to 50 nm per pulse for Kapton) and the lowest ablation threshold fluence (20 mJ cm$^{-2}$ for the triazene polymers compared to ~60 mJcm$^{-2}$ for Kapton) for selected wavelengths. The structure produced in TP (Fig. 7.22 (*top*)) with 308 nm irradiation are much sharper than those in Kapton$^{TM}$ (Fig. 7.22 (*bottom*)) and also no polymer debris is redeposited in and around the ablated structure in the case of the triazene polymer [98]. Kapton$^{TM}$ was chosen as commercially available reference because it has a similar $\alpha_{lin}$ at 308 nm. The absence of redeposited material for TP corresponds well with ns-shadowgraphy measurements, where it was shown that no solid products are produced for 308 nm irradiation of TP [99].

All data obtained for TP strongly suggest that photochemical reactions play an important role during UV laser ablation, but also that photothermal processes are important. This is confirmed by the presence of the thermal $N_2$ products in the TOF curves and from an analysis of the threshold fluence for very thin films, where a clear influence of the thermal conductivity of the substrate was detected [105]. Photothermal processes will also always

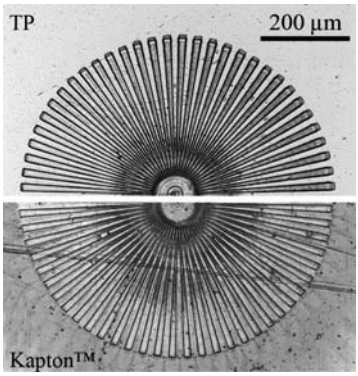


**Fig. 7.22.** SEM of Siemens Stars in TP (*top*) and Kapton™ (*bottom*), both produced with five laser pulses at 308 nm

be present if the polymer decomposes exothermically during a photochemical decomposition and if the quantum yield of the photochemical reaction is not equal to one (which is most of time the case). The ablation of polymers will therefore always be a photophysical process (a mixture of photochemical and photothermal processes), where the ratio between the two mechanisms is a function of the irradiation wavelength and the polymer. In addition photomechanical process, such as pressure produced by trapped gaseous ablation products or shock and acoustic waves in the polymer, take place [106] and can lead to a damage of the polymer and are probably most important for picosecond pulses [107, 108].

A more pronounced photochemical part is preferable for material structuring, as it leads to a more uniform decomposition of the polymer and results in less debris. Additionally large quantities of gaseous products are produced and less material is redeposited in and around the ablated area. The designed polymers such as the TP show a clear advantage over commercially available polymers.

## 7.3 Deposition of Thin Films Using UV Lasers

Thin polymers films of polymers are normally prepared by solvent-based methods, such as spin coating and master blading. Other techniques have the disadvantages that only complete layers with no lateral resolution are formed and that the polymers must be soluble in certain solvents, which are appropriate for these techniques. Requirements are that the solvent does not evaporate too fast, but still fast enough, and that relative large concentrations of the polymer (may be up to 15 wt.%) should be soluble. More problems exist for these techniques in the case of multilayers, which can only be realized for certain solvent systems and limits the number of polymers that can be used.

One technique that can be used to deposit layers with lateral resolution is ink jet printing, but in this case, the solvent may also be a problem, i.e., a high concentration solution with high viscosity must be used, and multilayers may also not be possible (depending on the solvents). Therefore "solvent-free" techniques, such as laser-based techniques have been developed.

Laser-based direct-writing and printing operations are finding increasing applications for precise surface micromodification techniques by either controlled ablation processes or the tailored deposition of complex materials. Several methods have been developed for the targeted deposition of a broad range of various materials applying lasers [109]. Among them, PLD can be used to grow films of inorganic [18, 19] or organic materials [15, 16, 110–113] on a substrate. A typical setup for PLD is shown in Fig. 7.23.

This method appears to be very limited, i.e., only a few polymers (PMMA, Teflon) have been deposited in this way (with UV laser irradiation) successfully. This is not really surprising, if we consider that UV photons will induce reactions and that the above described decomposition classification is valid. The previously described decomposition mechanisms show also clearly that only polymers which depolymerize, i.e., form the monomer upon UV laser irradiation, may be used for this approach. The deposited polymer films will most probably have a different molecular weight and weight distribution than the starting material, and may also contain decomposition products. One possible approach to deposit thin polymer films by PLD is the application of mid-infrared radiation, which is tuned to certain absorption bands of the polymer. This approach is called RIR-PLD (resonance-infra-red) and is described in detail in Chap. 8 by R. Haglund. A modified approach to PLD that is more

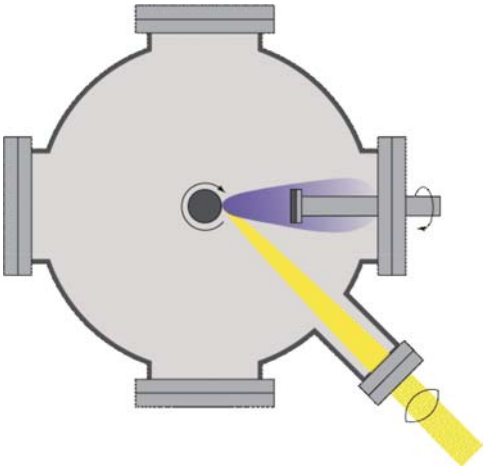

**Fig. 7.23.** Typical setup for PLD of organic or inorganic materials. The laser interacts with the moving target and vaporized the material to form a plasma (for inorganic materials) that is deposited on a substrate

gentle is MAPLE [110, 114], which uses in principle the same setup as PLD, with the main difference that the target consists of a frozen solution of the polymer. The laser is then used to vaporize the solvent that is removed by the pumps while the polymer chains are deposited intact on the substrate. This approach works of course only for polymer, which can be dissolved, and it should also work best when the laser is only/mainly absorbed by the solvent. The formation of high quality thin films is possible, although problems with the homogeneity of the films and trapped solvents exist. More details on MAPLE can be found in Chaps. 13 and 14 by A. Luches and I. Mihailescu.

Another versatile direct-writing method for the accurate microdeposition of a variety of different materials is based on LIFT techniques [21, 22, 115, 116], where the pressure increase from a vaporized material propels a transfer material onto a receiver. There are several different variations to this general approach:

1. Laser molecular implantation (LMI, scheme shown in Fig. 7.24).

For LMI a laser, which may be shaped by a mask, passes through a transparent substrate with a transparent polymer that is in contact with an absorbing polymer film containing the molecules that should be implanted, e.g., fluorescence probes, such as pyrene [117–119]. As absorbing polymer materials such as the triazene polymer can be utilized. It was possible with this approach to implant pyrene with a resolution given by the mask into the target polymer within a few 10s of nm. The disadvantage of this method is the limited number of polymers, which can be used (must be transparent with a quite low $T_g$) and that the implantation is only possible with a depth <100 nm.

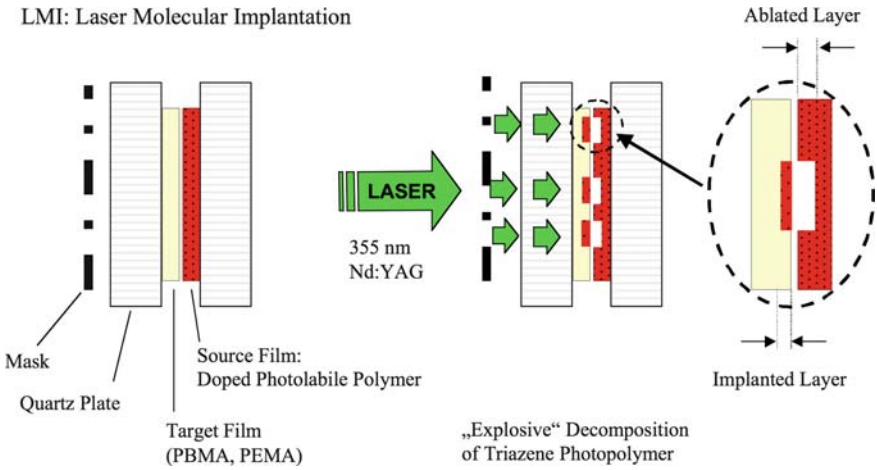


**Fig. 7.24.** Scheme of LMI

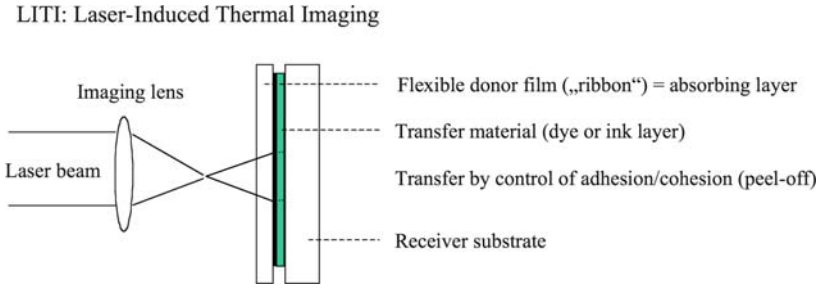


**Fig. 7.25.** Scheme of LITI

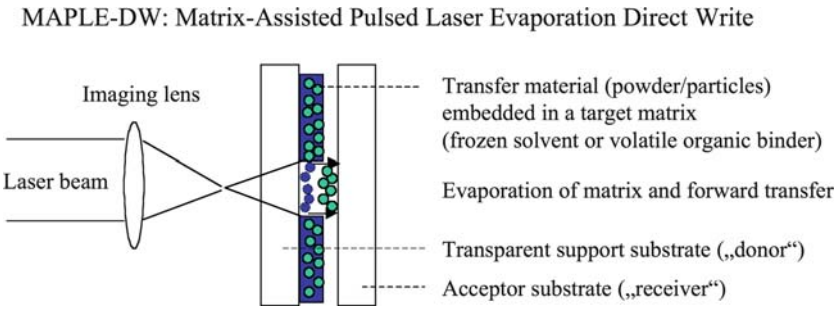


**Fig. 7.26.** Scheme of MAPLE-DW

2. Laser-induced thermal imaging (scheme shown in Fig. 7.25)

For LITI, typically IR lasers are used that are imaged through a flexible donor film onto an absorbing layer, which propels the material onto a receiver [120–122]. This may induce a thermal load to the transfer material. The thermal load may be detrimental to certain sensitive materials. Another key parameter to this technique is the control of adhesion and cohesion that can cause various problems.

3. Matrix-assisted pulsed laser evaporation direct write (MAPLE-DW, scheme shown in Fig. 7.26)

For MAPLE-DW the laser (mainly UV) is imaged through a transparent substrate onto the transfer material which is embedded in a matrix, e.g., frozen solvent or organic binder [110, 123–128]. The transfer material is then propelled over a gap to the receiver. There may be problems involved with the resolution of the transferred material (if it is liquid), a certain UV load, and that components of the matrix are also transferred.

4. Laser-induced forward transfer (LIFT, see Fig. 7.27).

For LIFT the UV laser is imaged through a transparent substrate on the transfer material and is transferred with or without a gap on the receiver [21, 22, 115, 116]. The main disadvantage of this method is the direct ablation

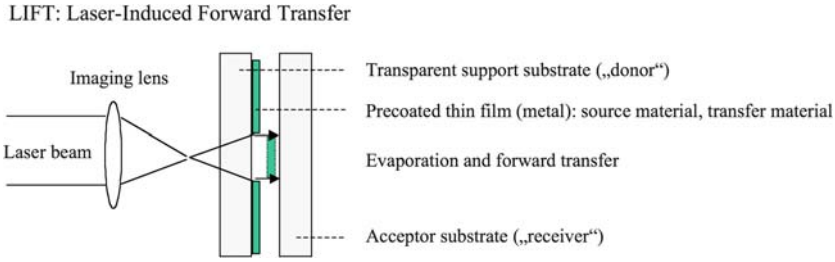


**Fig. 7.27.** Scheme of LIFT

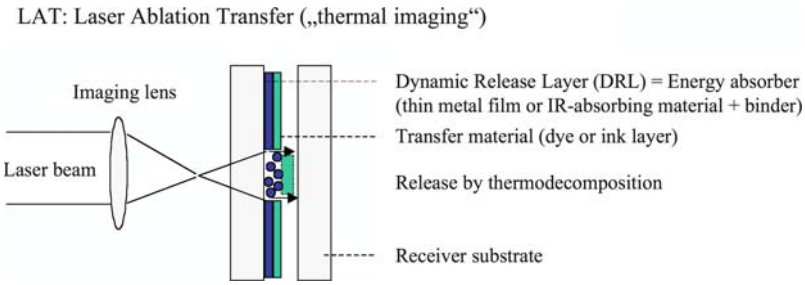


**Fig. 7.28.** Scheme of LAT

of the transfer material at the interface of the transfer. This may have a detrimental effect, i.e., decomposition, on the transfer material, especially if sensitive materials are used.

5. Laser ablation transfer (LAT, shown in Fig. 7.28).

In LAT an IR laser will be typically imaged onto an energy absorber which is also called dynamic release layer (DRL) or sacrificial layer [129–133]. The material is transferred over a gap onto the receiver, but the material may experience a thermal load and the fragments of the DRL that is often a metal may contaminate the transfer material. The use of thin intermediate films of metals (e.g., Ag, Au, Ti) or metal oxides (e.g., $TiO_2$) has been reported as absorbing layers for UV laser-based forward transfer applications of biomolecules [134–137] and cells [138]. This approach has then been called in the literature absorbing film assisted (AFA) LIFT [139–141] and Biological Laser Printing (BioLPTM) [142–146]. An alternative is the application of a thick polymer layer, which expands upon laser irradiation. This results in a “mechanical” transfer of the layer onto a receiver substrate [147].

In an attempt to overcome several of the above mentioned problems another variation of LIFT has been developed where UV lasers and a photosensitive, polymeric DRL is used. The advantage of this approach is that the control over the DRL thickness and laser fluence allows transferring sensitive material without any UV load as all photons are absorbed in the DRL layer. The complete composition of a polymeric DRL layer into gaseous fragments,

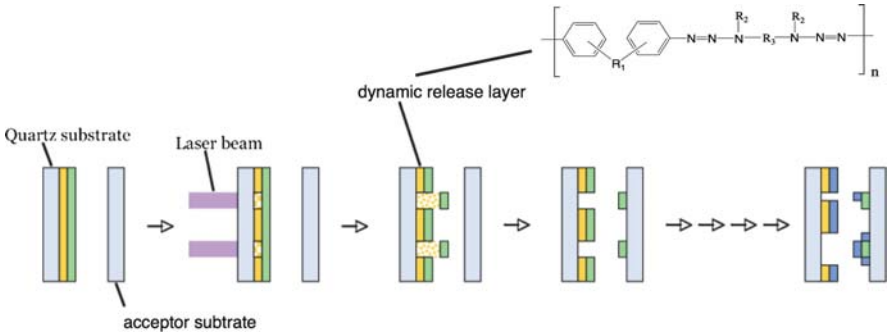


**Fig. 7.29.** Scheme of LIFT using a photosensitive DRL. The chemical structure of a DRL is included

as reported for the triazene polymers, allows then a contamination free transfer with ideally no thermal load of the material. A scheme of this approach is shown in Fig. 7.29, which also indicates the possibility to transfer multilayers.

From the chemical structure formula included in Fig. 7.29 it can be seen that two photocleavable aryltriazene (Ar–N=N–N–) chromophores per repeating unit are covalently incorporated into the polymer main chain. Exposure to UV irradiation causes a photolytic cleavage of the triazene chromophores, which leads to an irreversible evolution of elemental nitrogen and simultaneously to the fragmentation of the polymer into small molecules. Therefore, films of these photosensitive polymers proved to be excellently suitable for laser ablation applications since they can be cleanly ablated without carbonization or redeposition of debris already at fluences far below 100 mJ cm$^{-2}$ [6, 10, 148]. The laser-triggered photofragmentation process results in an abrupt volume expansion, which has been used to transfer a range of materials, i.e., metals and ceramics [149], and also sensitive materials such as neuroblasts (biomaterial) [150], polymers (OLED, optical light emitting diode materials) and bilayers of a metal with an OLED material (MEH-PPV) [151, 152]. With this approach (shown in Fig. 7.30 *left*) pixels of the OLED material were transferred with Al as electrode onto a transparent electrode (ITO).

The transferred OLED material was fully functional (see photo in Fig. 7.30 *right*) and the emission spectra revealed no indication of a thermal load (which would be indicative by a shoulder in the red), and gave the same slope efficiency as spin coated films [151–153]. This shows clearly that LIFT with a photosensitive polymeric DRL can be used to transfer sensitive material without thermal or UV load onto a receiver substrate with high lateral resolution.

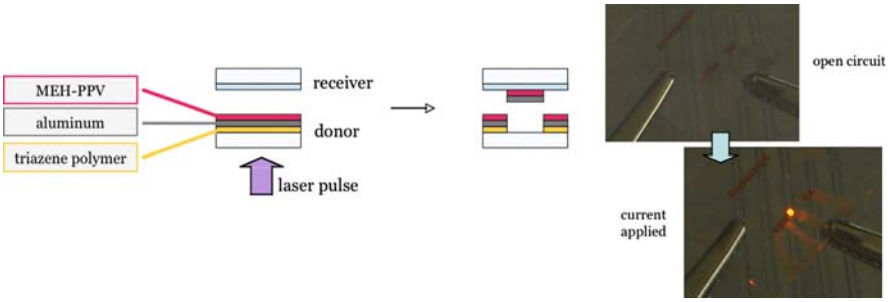


**Fig. 7.30.** Scheme of the bilayer transfer with DRL LIFT (*left*) and light emission of a transferred OLED (*right*)

## 7.4 Conclusion

UV laser ablation of polymers is a versatile method to structure polymers with high resolution. The mechanism of ablation is often discussed controversially, but it is necessary to keep in mind that polymers are complex systems with a wide variety of properties that can influence the ablation mechanism. Analyzing the data it appears that the ablation mechanism is a complex interrelated system, where photochemical and photothermal reactions are very important. The pressure jump, which is associated with the creation of small molecules and originates from both types of reaction, is also important for ablation. The importance of each effect is strongly dependent on the type of polymer, i.e., more photochemical features for specially designed polymers than for certain polyimides, the laser wavelengths (more photochemical features for shorter wavelengths), the pulse length and substrate.

UV laser ablation can also be utilized to deposit directly thin polymer films by PLD, but this is limited to certain polymers, i.e., polymers that decompose into the monomer upon decomposition. Alternative laser-based techniques, such as laser-induced forward transfer (LIFT), utilize the decomposition of a thin layer (either part of the material or in the form of a sacrificial layer) to transfer complete layers with high spatial resolution. This approach can be used to transfer pixels of sensitive materials to a substrate with a minimal thermal and UV load.

### Acknowledgments

Financial support of the Paul Scherrer Institut and the Swiss National Science Foundation to support parts of this work is gratefully acknowledged. Contributions from R. Fardel, M. Nagel, F. Nüesch, and L.Urech are also gratefully acknowledged.

## References


1. R. Srinivasan, V. Mayne-Banton, Appl. Phys. Lett. **41**, 576 (1982)
2. Y. Kawamura, K. Toyoda, S. Namba, Appl. Phys. Lett. **40**, 374 (1982)
3. R. Srinivasan, B. Braren, Chem. Rev. **89**, 1303 (1989)
4. D. Bäuerle, *Laser Processing and Chemistry*, 3rd edn. (Springer Verlag, Berlin, 2000)
5. S. Lazare, V. Granier, Laser Chem. **10**, 25 (1989)
6. T. Lippert, J.T. Dickinson, Chem. Rev. **103**, 453 (2003)
7. T. Lippert, in *Polymers and Light*, vol. 168, ed. by T. Lippert (Springer, Berlin, 2004) p. 51
8. P.E. Dyer, in *Photochemical Processing of Electronic Materials*, ed. by I.W. Boyd, R.B. Jackman (Academic, London, 1992) p. 360
9. N. Bityurin, B.S. Luk'yanchuk, M.H. Hong, T.C. Chong, Chem. Rev. **103**, 519 (2003)
10. T. Lippert, Plasma Process. Polym. **2**, 525 (2005)
11. N. Bityurin, Annu. Rep. Progr. Chem. C **101**, 216 (2005)
12. M. Karas, D. Bachmann, F. Hillenkamp, Anal. Chem. **57**, 2935 (1985)
13. R. Zenobi, R. Knochenmuss, Mass Spectrom. Rev. **17**, 337 (1998)
14. L.J. Radziemski, D.A. Cremers, *Laser-Induced Plasmas and Applications* (M. Dekker, New York, 1989)
15. G.B. Blanchet, Macromolecules **28**, 4603 (1995)
16. G.B. Blanchet, Chemtech **26**, 31 (1996)
17. W.B. Jiang, M.G. Norton, L. Tsung, J.T. Dickinson, J. Mater. Res. **10**, 1038 (1995)
18. R.W. Eason, *Pulsed Laser Deposition of Thin Films: Applications-Led Growth of Functional Materials* (John Wiley, Hoboken, NJ, 2007)
19. D.B. Chrisey, G.K. Hubler, *Pulsed Laser Deposition of Thin Films* (John Wiley, New York, 1994)
20. A. Pique, P. Wu, B.R. Ringeisen, D.M. Bubb, J.S. Melinger, R.A. McGill, D.B. Chrisey, Appl. Surf. Sci. **186**, 408 (2002)
21. J. Bohandy, B.F. Kim, F.J. Adrian, J. Appl. Phys. **60**, 1538 (1986)
22. K.D. Kyrkis, A.A. Andreadaki, D.G. Papazoglou, I. Zergioti, in *Recent Advances in Laser Processing of Materials*, vol. 241, ed. by J. Perrière, E. Millon, E. Fogarassy (Elsevier, Amsterdam, 2006) p. 213
23. H. Aoki (U.S. Patent 5736999, 1998)
24. R.S. Patel, T.A. Wassick, Proc. SPIE-Int. Soc. Opt. Eng. **2991**, 217 (1997)
25. G. Kopitkovas, L. Urech, T. Lippert, in *Recent Advances in Laser Processing of Materials,* ed. by E. Millon, J. Perriere, E. Fogarassy (Elsevier, Kidlington, 2006) p. 105
26. H. Klank, J.P. Kutter, O. Geschke, Lab Chip **2**, 242–246 (2002)
27. D. Snakenborg, H. Klank, J.P. Kutter, J. Micromech. Microeng. **14**, 182 (2004)
28. D. Gomez, F. Tekniker, I. Goenaga, I. Lizuain, M. Ozaita, Opt. Eng. **44**, 051105 (2005)
29. D.F. Farson, H.W. Choi, C.M. Lu, L.J. Lee, J. Laser Appl. **18**, 210 (2006)
30. S. Lazare, W.P. Guan, D. Drilhole, Appl. Surf. Sci. **96–98**, 605 (1996)
31. E.E. Ortelli, F. Geiger, T. Lippert, J. Wei, A. Wokaun, Macromolecules **33**, 5090 (2000)
32. P. Lemoine, W. Blau, A. Drury, C. Keely, Polymer **34**, 5020 (1993)

33. T. Lippert, A. Wokaun, J. Stebani, O. Nuyken, J. Ihlemann, Angew. Makromol. Chem. **213**, 127 (1993)
34. G. Bounos, A. Selimis, S. Georgiou, E. Rebollar, M. Castillejo, N. Bityurin, J. Appl. Phys. **100**, 114323 (2006)
35. E. Rebollar, G. Bounos, M. Oujja, S. Georgiou, M. Castillejo, J. Phys. Chem. B **110**, 16452 (2006)
36. R. Srinivasan, J. Appl. Phys. **70**, 7588 (1991)
37. R. Srinivasan, B. Braren, Appl. Phys. A **45**, 289 (1988)
38. P.E. Dyer, S.D. Jenkins, J. Sidhu, Appl. Phys. Lett. **52**, 1880 (1988)
39. P.E. Dyer, S.D. Jenkins, J. Sidhu, Appl. Phys. Lett. **49**, 453 (1986)
40. J. Wei, N. Hoogen, T. Lippert, O. Nuyken, A. Wokaun, J. Phys. Chem. B **105**, 1267 (2001)
41. F. Raimondi, S. Abolhassani, R. Brutsch, F. Geiger, T. Lippert, J. Wambach, J. Wei, A. Wokaun, J. Appl. Phys. **88**, 3659 (2000)
42. J. Krüger, W. Kautek, in *Polymers And Light*, vol. 168, ed. by T. Lippert (Springer, Berlin, 2004) p. 247
43. T. Dumont, R. Bischofberger, T. Lippert, A. Wokaun, Appl. Surf. Sci. **247**, 115 (2005)
44. T. Dumont, S. Lazare, T. Lippert, A. Wokaun, Appl. Phys. A **79**, 1271 (2004)
45. R. Srinivasan, B. Braren, D.E. Seeger, R.W. Dreyfus, Macromolecules **19**, 916 (1986)
46. R. Srinivasan, J. Appl. Phys. **73**, 2743 (1993)
47. J.E. Andrew, P.E. Dyer, D. Forster, P.H. Key, Appl. Phys. Lett. **43**, 717 (1983)
48. R. Srinivasan, B. Braren, J. Polym. Sci. A Polym. Chem. **22**, 2601 (1984)
49. R. Srinivasan, B. Braren, K.G. Casey, J. Appl. Phys. **68**, 1842 (1990)
50. S. Küper, M. Stuke, Appl. Phys. A **49**, 211 (1989)
51. S.V. Babu, G.C. D'Couto, F.D. Egitto, J. Appl. Phys. **72**, 692 (1992)
52. M. Himmelbauer, E. Arenholz, D. Bauerle, Appl. Phys. A **63**, 87 (1996)
53. G. Paraskevopoulos, D.L. Singleton, R.S. Irwin, R.S. Taylor, J. Appl.Phys. **70**, 1938 (1991)
54. R.S. Taylor, D.L. Singleton, G. Paraskevopoulos, Appl. Phys. Lett. **50**, 1779 (1987)
55. S. Küper, J. Brannon, K. Brannon, Appl. Phys. A **56**, 43 (1993)
56. S.R. Cain, J. Phys. Chem. **97**, 7572 (1993)
57. S.R. Cain, F.C. Burns, C.E. Otis, J. Appl. Phys. **71**, 4107 (1992)
58. G.C. D'Couto, S.V. Babu, J. Appl. Phys. **76**, 3052 (1994)
59. B. Lukyanchuk, N. Bityurin, M. Himmelbauer, N. Arnold, Nucl. Instrum. Methods Phys. Res. B **122**, 347 (1997)
60. N. Arnold, B. Luk'yanchuk, N. Bityurin, Appl. Surf. Sci. **129**, 184 (1998)
61. T.F. Deutsch, M.W. Geis, J. Appl. Phys. **54**, 7201 (1983)
62. E. Sutcliffe, R. Srinivasan, J. Appl. Phys. **60**, 3315 (1986)
63. G.D. Mahan, H.S. Cole, Y.S. Liu, H.R. Philipp, Appl. Phys. Lett. **53**, 2377 (1988)
64. V. Srinivasan, M.A. Smrtic, S.V. Babu, J. Appl. Phys. **59**, 3861 (1986)
65. H. Schmidt, J. Ihlemann, B. Wolff-Rottke, K. Luther, J. Troe, J. Appl. Phys. **83**, 5458 (1998)
66. B. Lukyanchuk, N. Bityurin, S. Anisimov, N. Arnold, D. Bauerle, Appl. Phys. A **62**, 397 (1996)
67. B. Lukyanchuk, N. Bityurin, S. Anisimov, D. Bauerle, Appl. Phys. A **57**, 367 (1993)

68. N. Bityurin, A. Malyshev, B. Luk'yanchuk, S. Anisimov, D. Bäuerle, Proc. SPIE-Int. Soc. Opt. Eng. **2802**, 103 (1996)
69. N. Bityurin, Appl. Surf. Sci. **139**, 354 (1999)
70. G.V. Treyz, R. Scarmozzino, R.M. Osgood, Appl. Phys. Lett. **55**, 346 (1989)
71. N. Arnold, N. Bityurin, Appl. Phys. A **68**, 615 (1999)
72. Y.G. Yingling, B.J. Garrison, J. Phys. Chem. B **109**, 16482 (2005)
73. Y.G. Yingling, B.J. Garrison, J. Phys. Chem. B **108**, 1815 (2004)
74. P.F. Conforti, M. Prasad, B.J. Garrison, Appl. Surf. Sci. **253**, 6386 (2007)
75. P.F. Conforti, M. Prasad, B.J. Garrison, J. Phys. Chem. C **111**, 12024 (2007)
76. M. Prasad, P.F. Conforti, B.J. Garrison, J. Appl. Phys. **101**, 103113 (2007)
77. M. Prasad, P.F. Conforti, B.J. Garrison, J. Chem. Phys. **127**, 084705 (2007)
78. M. Prasad, P.F. Conforti, B.J. Garrison, Y.G. Yingling, Appl. Surf. Sci. **253**, 6382 (2007)
79. Y.G. Yingling, B.J. Garrison, Appl. Surf. Sci. **253**, 6377 (2007)
80. Y.G. Yingling, L.V. Zhigilei, B.J. Garrison, J. Photochem. Photobiol. A Chem. **145**, 173 (2001)
81. L.V. Zhigilei, E. Leveugle, B.J. Garrison, Y.G. Yingling, M.I. Zeifman, Chem. Rev. **103**, 321 (2003)
82. Y.G. Yingling, B.J. Garrison, Chem. Phys. Lett. **364**, 237 (2002)
83. Y.G. Yingling, B.J. Garrison, Nucl. Instrum. Methods Phys. Res. B **202**, 188 (2003)
84. N. Bityurin, A. Malyshev, J. Appl. Phys. **92**, 605 (2002)
85. T. Lippert, A. Yabe, A. Wokaun, Adv. Mater. **9**, 105 (1997)
86. T. Lippert, J. Stebani, O. Nuyken, A. Stasko, A. Wokaun, J. Photochem. Photobiol. A Chem. **78**, 139 (1994)
87. O. Nuyken, J. Stebani, T. Lippert, A. Wokaun, A. Stasko, Macromol. Chem. Phys. **196**, 751 (1995)
88. A. Stasko, V. Adamcik, T. Lippert, A. Wokaun, J. Dauth, O. Nuyken, Makromol. Chem. Macromol. Chem. Phys. **194**, 3385 (1993)
89. O. Nuyken, J. Stebani, T. Lippert, A. Wokaun, A. Stasko, Macromol. Chem. Phys. **196**, 739 (1995)
90. T. Lippert, L.S. Bennett, T. Nakamura, H. Niino, A. Ouchi, A. Yabe, Appl. Phys. A **63**, 257 (1996)
91. T. Lippert, T. Nakamura, H. Niino, A. Yabe, Appl. Surf. Sci. **110**, 227 (1997)
92. T. Lippert, C. David, J.T. Dickinson, M. Hauer, U. Kogelschatz, S.C. Langford, O. Nuyken, C. Phipps, J. Robert, A. Wokaun, J. Photochem. Photobiol. A Chem. **145**, 145 (2001)
93. T. Lippert, A. Wokaun, S.C. Langford, J.T. Dickinson, Appl. Phys. A **69**, S655 (1999)
94. T. Lippert, S.C. Langford, A. Wokaun, G. Savas, J.T. Dickinson, J. Appl. Phys. **86**, 7116 (1999)
95. M. Hauer, J.T. Dickinson, S. Langford, T. Lippert, A. Wokaun, Appl. Surf. Sci. **197**, 791 (2002)
96. H. Furutani, H. Fukumura, H. Masuhara, J. Phys. Chem. **100**, 6871 (1996)
97. H. Furutani, H. Fukumura, H. Masuhara, S. Kambara, T. Kitaguchi, H. Tsukada, T. Ozawa, J. Phys. Chem. B **102**, 3395 (1998)
98. T. Lippert, J.T. Dickinson, M. Hauer, G. Kopitkovas, S.C. Langford, H. Masuhara, O. Nuyken, J. Robert, H. Salmio, T. Tada, K. Tomita, A. Wokaun, Appl. Surf. Sci. **197**, 746 (2002)

99. M. Hauer, D.J. Funk, T. Lippert, A. Wokaun, Appl. Surf. Sci. **208**, 107–112 (2003)
100. J. Bonse, S.M. Wiggins, J. Solis, T. Lippert, Appl. Surf. Sci. **247**, 440 (2005)
101. J. Bonse, S.M. Wiggins, J. Solis, T. Lippert, H. Sturm, Appl. Surf. Sci. **248**, 157 (2005)
102. E.C. Buruiana, T. Buruiana, H. Lenuta, T. Lippert, L. Urech, A. Wokaun, J. Polym. Sci. A Polym. Chem. **44**, 5271 (2006)
103. E.C. Buruiana, L. Hahui, T. Buruiana, L. Urech, T. Lippert, J. Photochem. Photobiol. A Chem. **195**, 337 (2008)
104. E.C. Buruiana, V. Melinte, T. Buruiana, T. Lippert, H. Yoshikawa, H. Mashuhara, J. Photochem. Photobiol. A Chemistry **171**, 261 (2005)
105. R. Fardel, M. Nagel, T. Lippert, F. Nuesch, A. Wokaun, B.S. Luk'yanchuk, Appl. Phys. A **90**, 661 (2008)
106. G. Paltauf, P.E. Dyer, Chem. Rev. **103**, 487 (2003)
107. D.E. Hare, D.D. Dlott, Appl. Phys. Lett. **64**, 715 (1994)
108. D.E. Hare, J. Franken, D.D. Dlott, J. Appl. Phys. **77**, 5950 (1995)
109. C.B. Arnold, P. Serra, A. Piqué, MRS Bull. **32**, 23 (2007)
110. D.B. Chrisey, A. Pique, R.A. McGill, J.S. Horwitz, B.R. Ringeisen, D.M. Bubb, P.K. Wu, Chem. Rev. **103**, 553 (2003)
111. X. Yang, Y. Tang, M. Yu, Q. Qin, Thin Solid Films **358**, 187 (2000)
112. B. Losekrug, A. Meschede, H.U. Krebs, Appl. Surf. Sci. **254**, 1312 (2007)
113. E. Suske, T. Scharf, H.U. Krebs, T. Junkers, M. Buback, J. Appl. Phys. **100**, 014906 (2006)
114. D.B. Chrisey, A. Pique, J. Fitz-Gerald, R.C.Y. Auyeung, R.A. McGill, H.D. Wu, M. Duignan, Appl. Surf. Sci. **154**, 593 (2000)
115. C. Germain, L. Charron, L. Lilge, Y.Y. Tsui, Appl. Surf. Sci. **253**, 8328 (2007)
116. A. Klini, A. Mourka, V. Dinca, C. Fotakis, F. Claeyssens, Appl. Phys. A **87**, 17 (2007)
117. H. Fukumura: J. Photochem. Photobiol. A Chem. **106**, 3 (1997)
118. H. Fukumura, Y. Kohji, K. Nagasawa, H. Masuhara, J. Am. Chem. Soc. **116**, 10304 (1994)
119. D.M. Karnakis, T. Lippert, N. Ichinose, S. Kawanishi, H. Fukumura, Appl. Surf. Sci. **129**, 781 (1998)
120. J.Y. Lee, S.T. Lee, Adv. Mater. **16**, 51 (2004)
121. H.P. Le, J. Imaging Sci. Technol. **42**, 49 (1998)
122. F. Pschenitzka, J.C. Sturm, Appl. Phys. Lett. **74**, 1913 (1999)
123. D.B. Chrisey, A. Piqué, J. Fitz-Gerald, R.C.Y. Auyeung, R.A. McGill, H.D. Wu, M. Duignan, Appl. Surf. Sci. **154–155**, 593 (2000)
124. J.M. Fitz-Gerald, H.D. Wu, A. Pique, J.S. Horwitz, R.C.Y. Auyeung, W. Chang, W.J. Kim, D.B. Chrisey, Integrated Ferroelectrics **29**, 13 (2000)
125. A. Pique, D.B. Chrisey, R.C.Y. Auyeung, J. Fitz-Gerald, H.D. Wu, R.A. McGill, S. Lakeou, P.K. Wu, V. Nguyen, M. Duignan, Appl. Phys. A **69**, S279 (1999)
126. A. Pique, R.A. McGill, D.B. Chrisey, D. Leonhardt, T.E. Mslna, B.J. Spargo, J.H. Callahan, R.W. Vachet, R. Chung, M.A. Bucaro, Thin Solid Films **356**, 536 (1999)
127. D.B. Chrisey, A. Pique, R. Modi, H.D. Wu, R.C.Y. Auyeung, H.D. Young, Appl. Surf. Sci. **168**, 345 (2000)
128. D. Young, R.C.Y. Auyeung, A. Pique, D.B. Chrisey, D.D. Dlott, Appl. Phys. Lett. **78**, 3169 (2001)

129. S.G. Koulikov, D.D. Dlott, J. Imaging Sci. Technol. **44**, 111 (2000)
130. I.Y.S. Lee, W.A. Tolbert, D.D. Dlott, M.M. Doxtader, D.M. Foley, D.R. Arnold, E.W. Ellis, J. Imaging Sci. Technol. **36**, 180 (1992)
131. W.A. Tolbert, I.Y.S. Lee, M.M. Doxtader, E.W. Ellis, D.D. Dlott, J. Imaging Sci. Technol. **37**, 411 (1993)
132. W.A. Tolbert, I.YS. Lee, X.N. Wen, D.D. Dlott, M.M. Doxtader, E.W. Ellis, J. Imaging Sci. Technol. **37**, 485 (1993)
133. G.R. Pinto, J. Imaging Sci. Technol. **38**, 565 (1994)
134. J.M. Fernandez-Pradas, M. Colina, P. Serra, J. Dominguez, J.L. Morenza, Thin Solid Films **453**, 27 (2004)
135. P. Serra, M. Colina, J.M. Fernandez-Pradas, L. Sevilla, J.L. Morenza, Appl. Phys. Lett. **85**, 1639 (2004)
136. P. Serra, J.M. Fernandez-Pradas, F.X. Berthet, M. Colina, J. Elvira, J.L. Morenza, Appl. Phys. A **79**, 949 (2004)
137. V. Dinca, E. Kasotakis, J. Catherine, A. Mourka, A. Mitraki, A. Popescu, M. Dinescu, M. Farsari, C. Fotakis, Appl. Surf. Sci. **254**, 1160 (2007)
138. B. Hopp, T. Smausz, N. Kresz, N. Barna, Z. Bor, L. Kolozsvari, D.B. Chrisey, A. Szabo, A. Nogradi, Tissue Eng. **11**, 1817 (2005)
139. B. Hopp, T. Smausz, Z. Antal, N. Kresz, Z. Bor, D.B. Chrisey, J. Appl. Phys. **96**, 3478 (2004)
140. B. Hopp, T. Smausz, N. Barna, C. Vass, Z. Antal, L. Kredics, D.B. Chrisey, J. Phys. D Appl. Phys. **38**, 833 (2005)
141. T. Smausz, B. Hopp, G. Kecskeméti, Z. Bor, Appl. Surf. Sci. **252**, 4738 (2006)
142. J.A. Barron, D.B. Krizman, B.R. Ringeisen, Ann. Biomed. Eng. **33**, 121 (2005)
143. J.A. Barron, R. Rosen, J. Jones-Meehan, B.J. Spargo, S. Belkin, B.R. Ringeisen, Biosens Bioelectron **20**, 246 (2004)
144. J.A. Barron, B.J. Spargo, B.R. Ringeisen, Appl. Phys. A **79**, 1027 (2004)
145. J.A. Barron, P. Wu, H.D. Ladouceur, B.R. Ringeisen, Biomed. Microdevices **6**, 139 (2004)
146. J.A. Barron, H.D. Young, D.D. Dlott, M.M. Darfler, D.B. Krizman, B.R. Ringeisen, Proteomics **5**, 4138 (2005)
147. N.T. Kattamis, P.E. Purnick, R. Weiss, C.B. Arnold, Appl. Phys. Lett. **91**, 171120 (2007)
148. T. Lippert, Adv. Polym. Sci. **168**, 51 (2004)
149. D.P. Banks, K. Kaur, R. Gazia, R. Fardel, M. Nagel, T. Lippert, R.W. Eason, Europhys. Lett. **83**, 38003 (2008)
150. A. Doraiswamy, R.J. Narayan, T. Lippert, L. Urech, A. Wokaun, M. Nagel, B. Hopp, M. Dinescu, R. Modi, R.C.Y. Auyeung, D.B. Chrisey, Appl. Surf. Sci. **252**, 4743 (2006)
151. R. Fardel, M. Nagel, F. Nusch, T. Lippert, A. Wokaun, Appl. Surf. Sci. **254**, 1322 (2007)
152. R. Fardel, M. Nagel, F. Nuesch, T. Lippert, A. Wokaun, Appl. Phys. Lett. **91**, 061103 (2007)
153. M. Nagel, R. Fardel, P. Feurer, M. Häberli, F. Nüesch, T. Lippert, A. Wokaun, Appl. Phys. A **92**, 781 (2008)